NUCL SCI TECH (2019) 30:110
https://doi.org/10.1007/s41365-019-0631-1

Comparison of experimental and theoretical radiation shielding parameters of several environmentally friendly materials

F. Akman[1] · O. Agar[2] · M. R. Kaçal[3] · M. I. Sayyed[4]

Received: 6 October 2018 / Revised: 13 March 2019 / Accepted: 31 March 2019 / Published online: 6 June 2019

Abstract In this study, the gamma radiation shielding features of several environmentally friendly materials were investigated. For this purpose, several attenuation parameters, such as the mass attenuation coefficient (μ/ρ), radiation protection efficiency (RPE), and effective atomic number (Z_{eff}) were determined experimentally and compared with numerical data obtained using WinXCom software. In the measurements, the emitted gamma photons were counted by a gamma spectrometer equipped with an HPGe detector using ^{22}Na, ^{54}Mn, ^{57}Co, ^{60}Co, ^{133}Ba, and ^{137}Cs radioactive point sources in the energy region of 81–1333 keV. The obtained results indicate that the μ/ρ and RPE values of the samples decrease with an increase in photon energy. The experimental values are in good agreement with those obtained using WinXCom software. The RPE and Z_{eff} results show that among the studied materials, the $NaY_{0.77}Yb_{0.20}Er_{0.03}F_4$ sample has the best gamma radiation shielding effectiveness.

✉ F. Akman
fakman@bingol.edu.tr

[1] Vocational School of Technical Sciences, Department of Electronic Communication Technology, Bingöl University, 12000 Bingöl, Turkey

[2] Department of Physics, Karamanoğlu Mehmetbey University, Karaman, Turkey

[3] Department of Physics, Arts and Sciences Faculty, Giresun University, 28100 Giresun, Turkey

[4] Department of Physics, Faculty of Science, University of Tabuk, Tabuk, Saudi Arabia

Keywords Greener products · Radiation shielding · Attenuation coefficient · WinXCom · Radiation protection efficiency

1 Introduction

Rare-earth elements (REEs) play an increasingly important role in the transition to a low-carbon economy. In addition, they possess a high quantum efficiency in the visible region [1]. Recovering REEs from secondary sources is remarkably rare due to the scarcity of RE-bearing minerals, which results in a limited supply of REEs on the global market [2]. As a result, waste phosphors have become an urban mining resource from which REEs, such as yttrium (Y), europium (Eu), dysprosium (Dy), terbium (Tb), and cerium (Ce), can be extracted [3]. There are many high-tech applications of REEs. For example, europium-doped barium magnesium aluminate ($BaMgAl_{10}O_{17}:Eu^{2+}$, BAM) is used in various high-resolution devices, including mercury-free lamps, field-emission displays (FEDs), light-emitting diodes (LEDs), and plasma display panels (PDPs). BAM, an attractive blue phosphor, offers excellent chromaticity, chemical stability, and high luminance efficiency under both ultraviolet (UV) and vacuum ultraviolet (VUV) excitations [4–6]. Terbium-doped cerium magnesium aluminate ($CeMgAl_{11}O_{19}$:Tb, CMAT) has been widely used as the green-emitting component in three-band lamps and has been studied for use in some PDPs [7, 8]. In particular, it is used in long-life and high-loading fluorescent lamps due to its high durability under intense UV radiation [9]. Sodium–yttrium–fluoride ($NaYF_4$), among all RE-doped fluoride host nanocrystals, is preferred for use in medical and biological fields due to

the noninvasive deep-tissue penetration of its radiation [10], its low toxicity [11], and its biocompatibility [12]. Finally, the incorporation of rare-earth ions, i.e., Eu^{2+}, Dy^{3+}, etc., into the lattice structure of afterglow phosphors both confers upon it the afterglow effect and introduces defects in crystal lattices [13].

Further, gamma radiation shielding features of REEs make them desirable for use in Pb (lead)-free radiation protection aprons due to health, environmental, and economic benefits of using substances that are less toxic than Pb for radiation protection. Moreover, a study of the radiation shielding features of REEs may aid in the design of new radiation protection materials made of non-toxic and green products. Recently, there has been an increasing demand for non-Pb (or non-toxic) materials that provide radiation protection. Some research has been performed on the high-energy attenuation performance of green and non-toxic materials [14–16]. Basic parameters, such as linear and mass attenuation coefficients, effective atomic number, and effective electron density yield important information about the radiation attenuation properties of these materials when matter and photons interact.

To the best of our knowledge, there are no studies in the literature on the radiation shielding performance of the green materials $NaY_{0.77}Yb_{0.20}Er_{0.03}F_4$, $Ba_{0.86}Eu_{0.14}MgAl_{10}O_{17}$, $Sr_{3.84}Eu_{0.06}Dy_{0.10}Al_{14}O_{25}$, $Ce_{0.63}Tb_{0.37}MgAl_{11}O_{19}$, and $Sr_{0.95}Eu_{0.02}Dy_{0.03}Al_2O_4$. The primary aim of this work was to experimentally evaluate the radiation shielding characteristics of these environmentally friendly products at different energies, i.e., between 81 and 1333 keV, and compare our results to the theoretical ones obtained using the WinXCom software.

2 Material and method

2.1 Experimental details

The spectroscopic pure materials were in the form of a powder and supplied by Sigma-Aldrich (St. Louis, MO, USA). All the materials had a purity of $\geq$ 99%. The particle size was 37 mm after being sieved to minimize the effects of the powder particle size on the results. To evaluate the gamma radiation shielding effectiveness, pellets with a diameter of 10 mm and thickness varying from 0.08 to 0.128 cm were produced by pressing the powder under a pressure of 10 ton cm^{-2} utilizing a manual hydraulic press after precisely determining the mass of the powder using a digital balance with an accuracy of 0.001 g. The evaluated samples consisted primarily of O, F, Na, Mg, Al, Sr, Y, Ba, Ce, Eu, Tb, Dy, Er, and Yb. The amounts of these elements in the samples were associated with the coding of $NaY_{0.77}Yb_{0.20}Er_{0.03}F_4$, $Ba_{0.86}Eu_{0.14}MgAl_{10}O_{17}$, $Sr_{3.84}Eu_{0.06}Dy_{0.10}Al_{14}O_{25}$, $Ce_{0.63}Tb_{0.37}MgAl_{11}O_{19}$, and $Sr_{0.95}Eu_{0.02}Dy_{0.03}Al_2O_4$, with densities of 3.46, 2.33, 2.61, 2.15, and 1.96 g/cm^3, respectively.

A high-purity germanium (HPGe) gamma-ray spectrometric system was used to measure the intensities of high-energy photons from several radioactive point sources: ^{133}Ba (81, 276, 303, 356 and 384 keV), ^{57}Co (121 and 136 keV), ^{137}Cs (662 keV), ^{60}Co (1173 and 1333 keV), ^{54}Mn (835 keV), and ^{22}Na (1275 keV). The diameter and thickness of the HPGe detector were 70 and 25 mm, respectively. The resolutions were 0.380, 0.585, and 1.8 keV at full width and 5.9, 122, and 1330 keV at full width half maximum (FWHM). During the measurements, the detector was kept at a temperature of − 196 °C by liquid nitrogen (N_2). The system's energy calibration was performed using the calibration sources ^{22}Na, ^{54}Mn, $^{57,60}Co$, ^{137}Cs, ^{133}Ba, ^{203}Hg, and ^{241}Am. A schematic of the experimental setup used in this study is given in Fig. 1. An absorbent material was placed between the radioactive point source and the detector. The data were analyzed with an ORTEC MAESTRO software package program [17, 18]. Using the Origin 7.5 program (demo), the net area counts were determined via the least-squares fitting method. Furthermore, the experimental uncertainties in the measurements were calculated according to the following equation [19, 20]:

$$\Delta\mu_{\mathrm{m}} = \frac{1}{\rho x}\sqrt{\left(\frac{\Delta I}{I}\right)^2 + \left(\frac{\Delta I_0}{I_0}\right)^2 + \ln\left(\frac{\Delta I}{I}\right)^2\left(\frac{\Delta\rho x}{\rho x}\right)^2}, \quad (1)$$

where ρ and x represent the density and thickness of the samples, respectively, $\Delta\rho x$ represents the uncertainty in mass per unit area, ΔI_0 and ΔI denote the uncertainties for I_0 and I, respectively.

2.2 Theoretical background

The linear attenuation (μ) of the materials to be tested followed the well-known exponential attenuation law:

$$\mu = -\frac{\ln\frac{I}{I_0}}{x}, \quad (2)$$

where I and I_0 denote the transmitted and original intensities, respectively, and x is the thickness (cm).

Using the density of any compound or mixture and μ, the mass attenuation coefficient (μ_{m}) was obtained [21]:

$$\mu_{\mathrm{m}} = \frac{\mu}{\rho} = \sum w_i\left(\frac{\mu}{\rho}\right)_i, \quad (3)$$

where w_i denotes the weight fraction for the individual element in any material. The μ_{m} value for the tested samples was computed for a particular energy range using the WinXCom program based on the mixture rule [22] (Eq. 3), which is expressed in cm^2/g.

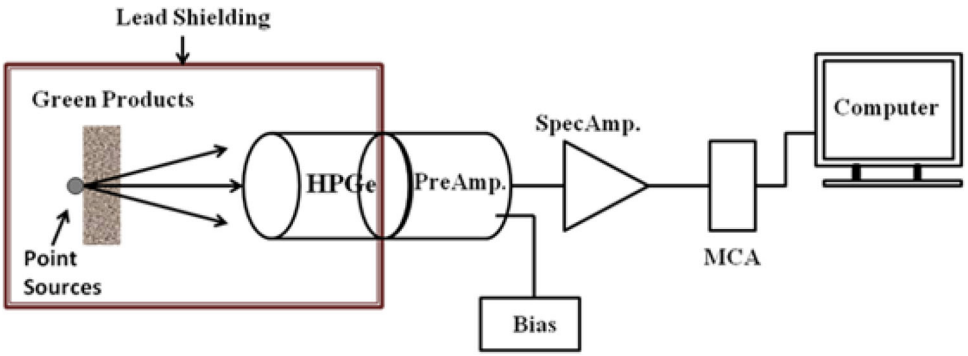

Fig. 1 Schematic of the experimental system (revised from [38]), where the distances between the gamma-ray source and the sample, and the window the of HPGe detector and the sample are 1 cm and 14 cm, respectively

It derived many parameters, such as total molecular ($\sigma_{t,m}$), atomic (σ_a) and electronic cross sections (σ_e) using the mass attenuation coefficient. $\sigma_{t,m}$ parameter was obtained as follows [23, 24]:

$$\sigma_{t,m} = \frac{1}{N_A}\left(\mu/\rho\right)_{samp.} \sum_i (n_i A_i), \tag{4}$$

where N_A is the Avogadro constant, A_i and n_i denote the atomic weight and the element number of the ith element in the material, respectively. It is expressed in cm^2/molecule.

σ_a, expressed in cm^2/atom, was determined as follows [25, 26]:

$$\sigma_a = \sigma_{t,m} / \sum_i n_i, \tag{5}$$

σ_e was calculated by the following relation [27, 28]:

$$\sigma_e = \frac{1}{N}\sum_i \left(\frac{\mu}{\rho}\right)_i \frac{f_i A_i}{Z_i}, \tag{6}$$

where f_i and Z_i represent the fractional abundance and the atomic number of the individual element, respectively. It is expressed in cm^2/electron.

The effective atomic number (Z_{eff}), a dimensionless quantity, was calculated from σ_a and σ_e [29]:

$$Z_{eff} = \frac{\sigma_a}{\sigma_e}. \tag{7}$$

The radiation protection efficiency (RPE) of any material was determined as follows [30]:

$$\text{RPE}\ (\%) = \left(1 - \frac{I}{I_0}\right) \times 100, \tag{8}$$

where 100 is the coefficient of percent efficiency (%).

3 Results and discussion

The experimental values of μ/ρ for $NaY_{0.77}Yb_{0.20}Er_{0.03}F_4$, $Ba_{0.86}Eu_{0.14}MgAl_{10}O_{17}$, $Sr_{3.84}Eu_{0.06}Dy_{0.10}Al_{14}O_{25}$, $Ce_{0.63}Tb_{0.37}MgAl_{11}O_{19}$, and $Sr_{0.95}Eu_{0.02}Dy_{0.03}Al_2O_4$ at several photon energies (ranging from 81 to 1333 keV) using several radioactive point sources were measured and are listed in Table 1. The experimental μ/ρ value was compared with the theoretical one calculated using the WinXCom computer software [22] to confirm the accuracy of the experimental results of this study. The experimental and theoretical results were plotted and the graphs are shown in Fig. 2. Table 1 and Fig. 2 show that the experimental and theoretical μ/ρ values decrease as the photon energy increases. The trend of μ/ρ with energy can understand photon interaction mechanisms, namely the photoelectric effect (PE), Compton scattering (CS), and pair production (PP), as discussed in the previous studies [26, 30, 31]. At lower energies, the changes in the attenuation coefficients are due changes in the PE as the energy varies, whereas at medium energies, they are dependent on changes in the CS effect. Furthermore, $NaY_{0.77}Yb_{0.20}Er_{0.03}F_4$, which includes two elements with a high Z value (Yb, $Z = 70$ and Eu, $Z = 68$), has the highest μ/ρ value among all of the studied materials. However, $NaY_{0.77}Yb_{0.20}Er_{0.03}F_4$ is twice as expensive as any of the other materials. Although the mass attenuation coefficient of $Sr_{3.84}Eu_{0.06}Dy_{0.10}Al_{14}O_{25}$ is lower than those of the other samples, it is the least expensive among the samples. Table 1 and Fig. 2 show that the experimental and theoretical μ/ρ values are in good agreement. However, the small differences between the experimental and theoretical data are due to uncertainties in the system, thickness of the sample, original intensity (I_0), and attenuated photon intensity (I) [25]. The uncertainties in attenuation coefficient values are $< \pm$ 3.97%.

Table 2 presents the mass attenuation coefficient values for Al, Fe, and ordinary concrete [32] calculated by WinXCom in comparison with the experimental values. From Tables 1 and 2, it can be seen that the μ/ρ values for all studied samples are higher than that of Al in the energy range of 81–511 keV. Moreover, Fe has a higher μ/ρ value than all the experimental samples in the energy range of 81–303 keV. We note that all the samples have higher μ/ρ values than ordinary concrete at low energies ($E < 356$ keV), while the μ/ρ value of ordinary concrete is

Table 1 Experimental and theoretical mass attenuation coefficient values for selected greener alternative products

Energy (keV)	$NaY_{0.77}Yb_{0.20}Er_{0.03}F_4$		$Ba_{0.86}Eu_{0.14}MgAl_{10}O_{17}$		$Sr_{3.84}Eu_{0.06}Dy_{0.10}Al_{14}O_{25}$		$Ce_{0.63}Tb_{0.37}MgAl_{11}O_{19}$		$Sr_{0.95}Eu_{0.02}Dy_{0.03}Al_2O_4$	
	Exp.	WinX.	Exp.	WinX.	Exp.	WinX.	Exp.	WinX.	Exp.	WinX.
81	0.5767 ± 0.0062	0.5924	0.3173 ± 0.0034	0.3126	0.3043 ± 0.0033	0.3110	0.3283 ± 0.0035	0.3230	0.3984 ± 0.0043	0.3871
122	0.2799 ± 0.0040	0.2771	0.1979 ± 0.0029	0.1904	0.1815 ± 0.0026	0.1877	0.1848 ± 0.0027	0.1944	0.2203 ± 0.0032	0.2110
136	0.2447 ± 0.0097	0.2350	0.1808 ± 0.0066	0.1727	0.1620 ± 0.0058	0.1703	0.1823 ± 0.0066	0.1757	0.1796 ± 0.0065	0.1870
161	0.1954 ± 0.0054	0.1908	0.1479 ± 0.0031	0.1529	0.1528 ± 0.0037	0.1510	0.1601 ± 0.0036	0.1550	0.1596 ± 0.0037	0.1613
276	0.1210 ± 0.0044	0.1184	0.1149 ± 0.0041	0.1133	0.1179 ± 0.0043	0.1123	0.1119 ± 0.0040	0.1139	0.1182 ± 0.0042	0.1142
303	0.1169 ± 0.0026	0.1117	0.1060 ± 0.0024	0.1086	0.1118 ± 0.0025	0.1077	0.1103 ± 0.0024	0.1091	0.1062 ± 0.0024	0.1091
356	0.0978 ± 0.0011	0.1016	0.0962 ± 0.0011	0.1009	0.1021 ± 0.0012	0.1002	0.0974 ± 0.0011	0.1013	0.0967 ± 0.0011	0.1009
384	0.0952 ± 0.0028	0.0975	0.0948 ± 0.0027	0.0976	0.0944 ± 0.0028	0.0969	0.1005 ± 0.0028	0.0979	0.1008 ± 0.0028	0.0974
511	0.0810 ± 0.0010	0.0841	0.0883 ± 0.0011	0.0859	0.0839 ± 0.0010	0.0854	0.0834 ± 0.0010	0.0861	0.0822 ± 0.0010	0.0854
662	0.0754 ± 0.0009	0.0740	0.0739 ± 0.0009	0.0764	0.0734 ± 0.0009	0.0760	0.0742 ± 0.0009	0.0765	0.0771 ± 0.0009	0.0758
835	0.0692 ± 0.0018	0.0660	0.0712 ± 0.0020	0.0685	0.0715 ± 0.0020	0.0681	0.0697 ± 0.0020	0.0686	0.0700 ± 0.0020	0.0679
1173	0.0551 ± 0.0007	0.0556	0.0555 ± 0.0007	0.0579	0.0550 ± 0.0007	0.0576	0.0599 ± 0.0007	0.0580	0.0596 ± 0.0007	0.0574
1275	0.0556 ± 0.0006	0.0532	0.0571 ± 0.0007	0.0555	0.0574 ± 0.0007	0.0552	0.0579 ± 0.0007	0.0555	0.0537 ± 0.0006	0.0550
1333	0.0514 ± 0.0006	0.0520	0.0528 ± 0.0006	0.0542	0.0555 ± 0.0006	0.0539	0.0521 ± 0.0006	0.0543	0.0562 ± 0.0006	0.0537

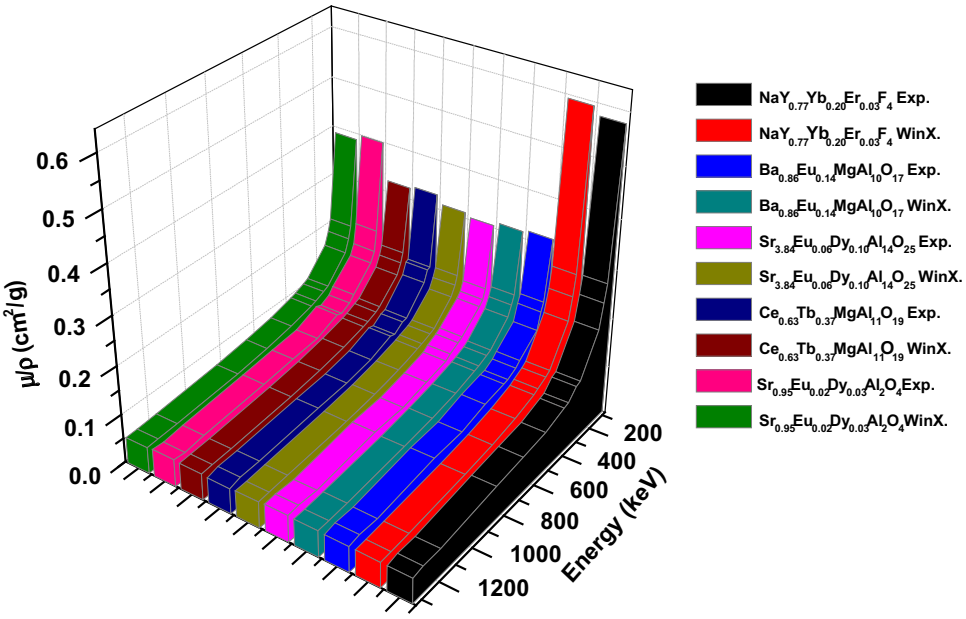

Fig. 2 (Color online) Mass attenuation coefficients for the investigated materials

Table 2 Mass attenuation coefficient for Al, Fe, and ordinary concrete

Energy (keV)	Al	Fe	Ordinary concrete
81	0.1996	0.5787	0.2022
122	0.1520	0.2623	0.1567
136	0.1441	0.2233	0.1490
161	0.1337	0.1808	0.1386
276	0.1077	0.1156	0.1122
303	0.1038	0.1092	0.1082
356	0.0973	0.0999	0.1015
384	0.0943	0.0960	0.0984
511	0.0837	0.0833	0.0873
662	0.0747	0.0735	0.0779
835	0.0670	0.0656	0.0700
1173	0.0568	0.0553	0.0593
1275	0.0544	0.0530	0.0568
1333	0.0532	0.0518	0.0555

higher than those of the samples at high energies ($E > 384$ keV).

To test the effectiveness of any absorber in the attenuation of gamma photons, the RPE (%) was calculated using the measured original (I_0) and attenuated photon intensities (I); our experimental values are listed in Table 3. The graph of RPE versus energy is shown in Fig. 3. As seen in Table 3 and Fig. 3, the RPE values decrease with an increase in photon energy. The RPE values of $NaY_{0.77}Yb_{0.20}Er_{0.03}F_4$, $Ba_{0.86}Eu_{0.14}MgAl_{10}O_{17}$, and $Sr_{3.84}Eu_{0.06}Dy_{0.10}Al_{14}O_{25}$ are quite close to each other at high energies ($E > 200$ keV), while $NaY_{0.77}Yb_{0.20}Er_{0.03}F_4$ has maximum RPE values of 14.75%, 7.45%, 6.55%, and 5.27% at energies of 81, 122, 136, and 161 keV, respectively.

Figure 4 contains a plot of the Z_{eff} of the five samples versus photon energy in the photon energy range of 0.015–10 MeV, obtained using the Auto-Z_{eff} program [33]. The size of Z_{eff} values plotted in the figure can be explained by considering the three types of photon scattering in matter. In the lower energy region, the values of Z_{eff} for all samples are the highest, primarily due to the photoelectric interaction mechanism, as shown in Fig. 4, and the effective cross section for this process depends directly upon the atomic number as Z^4 and the photon energy as $E^{-3.5}$ for any absorber. Apparently, Z_{eff} reduces exponentially with increasing photon energy up to about 800 keV, and then Z_{eff} values are almost constant. This is because the cross section for Compton scattering is related to the atomic number and the energy as Z and E^{-1}, respectively. In this high energy region, Compton scattering is the most important interaction process. From Fig. 4, we see that the Z_{eff} of $NaY_{0.77}Yb_{0.20}Er_{0.03}F_4 > Z_{eff}$ of $Sr_{3.84}Eu_{0.06}Dy_{0.10}Al_{14}O_{25} > Z_{eff}$ of $Ce_{0.63}Tb_{0.37}MgAl_{11}O_{19} > Z_{eff}$ of $Ba_{0.86}Eu_{0.14}MgAl_{10}O_{17} > Z_{eff}$ of $Sr_{0.95}Eu_{0.02}Dy_{0.03}Al_2O_4$. The high Z_{eff} values of $NaY_{0.77}Yb_{0.20}Er_{0.03}F_4$ are due to the presence of elements with high atomic number. We note that the graphs of Z_{eff} values for all samples have discontinuities due to photoelectric absorption near the K-, L-, and M-absorption edges of some elements at low energies (see Table 4). These results are in good agreement with the results for various glass systems obtained by El-Mallawany et al. [34], Kaur et al. [35], and Chanthima and Kaewkhao [36] and with the results for several smart polymer materials reported by Sayyed [37].

Table 3 Experimental radiation protection efficiency values for selected samples

Energy (keV)	$NaY_{0.77}Yb_{0.20}Er_{0.03}F_4$	$Ba_{0.86}Eu_{0.14}MgAl_{10}O_{17}$	$Sr_{3.84}Eu_{0.06}Dy_{0.10}Al_{14}O_{25}$	$Ce_{0.63}Tb_{0.37}MgAl_{11}O_{19}$	$Sr_{0.95}Eu_{0.02}Dy_{0.03}Al_2O_4$
81	14.75 ± 0.05	10.50 ± 0.04	9.66 ± 0.04	6.15 ± 0.02	8.08 ± 0.03
122	7.45 ± 0.08	6.69 ± 0.07	5.88 ± 0.06	3.51 ± 0.04	4.55 ± 0.05
136	6.55 ± 0.25	6.13 ± 0.22	5.27 ± 0.18	3.47 ± 0.12	3.73 ± 0.13
161	5.27 ± 0.13	5.04 ± 0.09	4.97 ± 0.11	3.05 ± 0.06	3.32 ± 0.07
276	3.29 ± 0.11	3.94 ± 0.13	3.86 ± 0.13	2.14 ± 0.07	2.47 ± 0.09
303	3.19 ± 0.06	3.64 ± 0.07	3.66 ± 0.07	2.11 ± 0.04	2.22 ± 0.04
356	2.67 ± 0.02	3.31 ± 0.02	3.35 ± 0.02	1.87 ± 0.01	2.03 ± 0.01
384	2.60 ± 0.07	3.26 ± 0.09	3.10 ± 0.09	1.93 ± 0.05	2.11 ± 0.06
511	2.22 ± 0.01	3.04 ± 0.02	2.76 ± 0.02	1.60 ± 0.01	1.72 ± 0.01
662	2.07 ± 0.01	2.55 ± 0.02	2.42 ± 0.02	1.43 ± 0.01	1.62 ± 0.01
835	1.90 ± 0.05	2.46 ± 0.07	2.36 ± 0.06	1.34 ± 0.04	1.47 ± 0.04
1173	1.51 ± 0.01	1.92 ± 0.01	1.82 ± 0.01	1.15 ± 0.01	1.25 ± 0.01
1275	1.53 ± 0.01	1.98 ± 0.01	1.90 ± 0.01	1.11 ± 0.01	1.13 ± 0.01
1333	1.41 ± 0.01	1.83 ± 0.01	1.84 ± 0.01	1.00 ± 0.01	1.18 ± 0.01

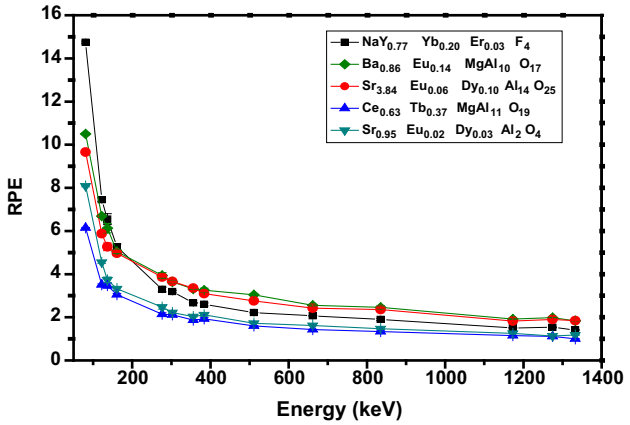

Fig. 3 (Color online) Radiation protection efficiencies of the samples versus energy

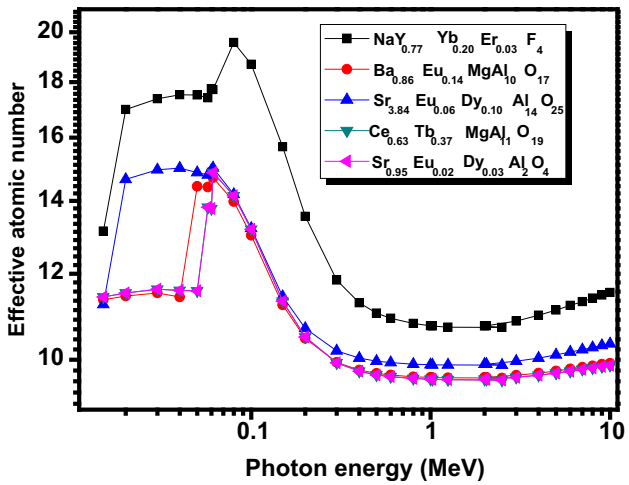

Fig. 4 (Color online) Effective atomic number of the five samples

4 Conclusion

The shielding performances of five compounds containing REEs, namely $NaY_{0.77}Yb_{0.20}Er_{0.03}F_4$, $Ba_{0.86}Eu_{0.14}MgAl_{10}O_{17}$, $Sr_{3.84}Eu_{0.06}Dy_{0.10}Al_{14}O_{25}$, $Ce_{0.63}Tb_{0.37}MgAl_{11}O_{19}$, and $Sr_{0.95}Eu_{0.02}Dy_{0.03}Al_2O_4$, were studied at photon energies between 81 and 1333 keV. The values of μ/ρ, RPE, and Z_{eff} were experimentally and theoretically evaluated. The obtained values indicate that Z_{eff} is dependent on gamma-ray energy intensity as well as the interaction mechanism. The Z_{eff} values peak when the photon energy values are low because the photoelectric effect around the K-, L-, and M- absorption edges of the samples dominates. Results for RPE and Z_{eff} also revealed that among the five materials studied, $NaY_{0.77}Yb_{0.20}Er_{0.03}F_4$ offers the best gamma-ray radiation protection. The obtained data may be helpful in various radiation shielding applications.

Table 4 Photon energies (in keV) of absorption edges of the elements under investigation [39]

Element	Z	K	L1	L2	L3	M1	M2	M3	M4	M5
Na	11	1.072	–	–	–	–	–	–	–	–
Mg	12	1.305	–	–	–	–	–	–	–	–
Al	13	1.559	–	–	–	–	–	–	–	–
Sr	38	16.105	2.216	2.007	1.940	–	–	–	–	–
Y	39	17.038	2.373	2.156	2.080	–	–	–	–	–
Ba	56	37.440	5.989	5.624	5.247	1.293	1.137	1.062	–	–
Ce	58	40.443	6.549	6.164	5.723	1.435	1.273	1.185	–	–
Eu	63	48.519	8.052	7.617	6.977	1.800	1.614	1.481	1.161	1.131
Tb	65	51.996	8.708	8.252	7.514	1.968	1.768	1.611	1.275	1.241
Dy	66	53.789	9.046	8.581	7.790	2.047	1.842	1.676	1.322	1.295
Er	68	57.486	9.751	9.264	8.357	2.207	2.006	1.812	1.453	1.409
Yb	70	61.332	10.486	9.978	9.944	2.398	2.173	1.950	1.576	1.528

References

1. M. Humphries, *Rare Earth Elements: The Global Supply Chain*. https://fas.org/sgp/crs/natsec/R41347.pdf. Accessed 15 Sept 2018
2. K. Binnemans, P.T. Jones, B. Blanpain et al., Recycling of rare earths: a critical review. J. Clean. Prod. **51**(1–22), 2013 (2013). https://doi.org/10.1016/j.jclepro.2012.12.037
3. T. Hirajima, K. Sasaki, A. Bissombolo et al., Feasibility of an efficient recovery of rare earth-activated phosphors from waste fluorescent lamps through dense-medium centrifugation. Sep. Purif. Technol. **44**(3), 197–204 (2005). https://doi.org/10.1016/j.seppur.2004.12.014
4. R. Shanker, A.F. Khan, R. Kumar et al., Understanding and arresting degradation in highly efficient blue emitting $BaMgAl_{10}O_{17}:Eu^{2+}$ phosphor—a longstanding technological problem. J. Lumin. **143**, 173–180 (2013). https://doi.org/10.1016/j.jlumin.2013.04.021
5. V. Singh, R.P.S. Chakradhar, J.L. Rao et al., EPR and photoluminescence properties of combustion-synthesized $ZnAl_2O_4:Cr^{3+}$ phosphors. J. Mater. Sci. **46**(7), 2331–2337 (2011). https://doi.org/10.1007/s10853-010-5078-z
6. C.W. Won, H.H. Nersisyan, H.I. Won et al., Synthesis of nano-size $BaMgAl_{10}O_{17}:Eu^{2+}$ blue phosphor by a rapid exothermic reaction. J. Lumin. **130**(4), 678–681 (2010). https://doi.org/10.1016/j.jlumin.2009.11.017
7. B.M.J. Smets, Phosphors based on rare-earths, a new era in fluorescent lighting. Mater. Chem. Phys. **16**(3–4), 283–299 (1987). https://doi.org/10.1016/0254-0584(87)90103-9
8. J. Zhang, Z. Zhang, Z. Tang et al., Mn^{2+} luminescence in (Ce, Tb)$MgAl_{11}O_{19}$ phosphor. Mater. Chem. Phys. **72**(1), 81–84 (2001). https://doi.org/10.1016/S0254-0584(01)00301-7
9. B. Park, S. Lee, J. Kang et al., Single-step solid-state synthesis of $CeMgAl_{11}O_{19}$:Tb phosphor. Bull. Korean Chem. Soc. **28**(9), 1467–1471 (2007). https://doi.org/10.5012/bkcs.2007.28.9.1467
10. Q. Liu, W. Feng, T. Yang et al., Upconversion luminescence imaging of cells and small animals. Nat. Protoc. **8**(10), 2033–2044 (2013). https://doi.org/10.1038/nprot.2013.114
11. J.C. Zhou, Z.L. Yang, W. Dong et al., Bioimaging and toxicity assessments of near-infrared upconversion luminescent $NaYF_4$:Yb, Tm nanocrystals. Biomaterials **32**(34), 9059–9067 (2011). https://doi.org/10.1016/j.biomaterials.2011.08.038
12. J. Shan, J. Chen, J. Meng et al., Biofunctionalization, cytotoxicity, and cell uptake of lanthanide doped hydrophobically ligated $NaYF_4$ upconversion nanophosphors. J. Appl. Phys. **104**(9), 094308 (2008). https://doi.org/10.1063/1.3008028
13. D. Dacyl, D. Uhlich, T. Jüstel, The effect of calcium substitution on the afterglow of Eu^{2+}/Dy^{3+}doped $Sr_4Al_{14}O_{25}$. Cent. Eur. J. Chem. **7**(2), 164–167 (2009). https://doi.org/10.2478/s11532-009-0017-z
14. L.B.T. La, C. Leatherday, Y.K. Leong et al., Green lightweight lead-free Gd_2O_3/epoxy nanocomposites with outstanding X-ray attenuation performance. Compos. Sci. Technol. **163**, 89–95 (2018). https://doi.org/10.1016/j.compscitech.2018.05.018
15. J.P. McCaffrey, F. Tessier, H. Shen, Radiation shielding materials and radiation scatter effects for interventional radiology (IR) physicians. Med. Phys. **39**(7), 4537–4546 (2012). https://doi.org/10.1118/1.4730504
16. G.J. Scuderi, G.V. Brusovanik, D.R. Campbell et al., Evaluation of on-lead-based protective radiological material in spinal surgery. Spine J. **6**(5), 577–582 (2006). https://doi.org/10.1016/j.spinee.2005.09.010
17. Maestro. https://www.ortec-online.com/products/application-software/maestro-mca. Accessed 15 Sept 2018
18. O. Agar, I. Boztosun, C. Segebade, Multielemental analysis of some soils in Karaman by PAA using a cLINAC. Appl. Radiat. Isot. **122**, 57–62 (2017). https://doi.org/10.1016/j.apradiso.2017.01.011
19. F. Akman, I.H. Geçibesler, M.I. Sayyed et al., Determination of some useful radiation interaction parameters for waste foods. Nucl. Eng. Technol. **50**(6), 944–949 (2018). https://doi.org/10.1016/j.net.2018.05.007
20. H.S. Mann, G.S. Brar, K.S. Mann et al., Experimental investigation of clay fly ash bricks for gamma-ray shielding. Nucl. Eng. Technol. **48**(5), 1230–1236 (2016). https://doi.org/10.1016/j.net.2016.04.001
21. J.H. Hubbell, Photon mass attenuation and energy-absorption coefficients. Int. J. Appl. Radiat. Isot. **33**(11), 1269–1290 (1982). https://doi.org/10.1016/0020-708X(82)90248-4
22. L. Gerward, N. Guilbert, K.B. Jensen et al., WinXCom—a program for calculating X-ray attenuation coefficients. Radiat. Phys. Chem. **71**(3), 653–654 (2004). https://doi.org/10.1016/j.radphyschem.2004.04.040
23. M.I. Sayyed, Bismuth modified shielding properties of zinc borotellurite glasses. J. Alloys Compd. **688**, 111–117 (2016). https://doi.org/10.1016/j.jallcom.2016.07.153
24. F. Akman, R. Durak, M.F. Turhan et al., Studies on effective atomic numbers, electron densities from mass attenuation coefficients near the K edge in some samarium compounds. Appl. Radiat. Isot. **101**, 107–113 (2015). https://doi.org/10.1016/j.apradiso.2015.04.001

25. F. Akman, M.R. Kaçal, F. Akman et al., Determination of effective atomic numbers and electron densities from mass attenuation coefficients for some selected complexes containing lanthanides. Can. J. Phys. **95**, 1005–1011 (2017). https://doi.org/10.1139/cjp-2016-0811
26. M.I. Sayyed, H.O. Tekin, O. Kılıcoglu et al., Shielding features of concrete types containing sepiolite mineral: comprehensive study on experimental, XCOM and MCNPX results. Results Phys. **11**, 40–45 (2018). https://doi.org/10.1016/j.rinp.2018.08.029
27. C. Eke, O. Agar, C. Segebade et al., Attenuation properties of radiation shielding materials such as granite and marble against γ-ray energies between 80 and 1350 keV. Radiochim. Acta **105**(10), 851–863 (2017). https://doi.org/10.1515/ract-2016-2690
28. F. Akman, R. Durak, M.R. Kacal et al., Study of absorption parameters around the K edge for selected compunds of Gd. X-Ray Spectrom. **45**(2), 103–110 (2016). https://doi.org/10.1002/xrs.2676
29. O. Agar, M.I. Sayyed, F. Akman et al., An extensive investigation on gamma ray shielding features of Pd/Ag-based alloys. Nucl. Eng. Technol. (2019). https://doi.org/10.1016/j.net.2018.12.014
30. M.I. Sayyed, Y. Elmahroug, B.O. Elbashir et al., Gamma-ray shielding properties of zinc oxide soda lime silica glasses. J. Mater. Sci. Mater. Electron. **28**(5), 4064–4074 (2017). https://doi.org/10.1007/s10854-016-6022-z
31. L. Shamshad, G. Rooh, P. Limkitjaroenporn et al., A comparative study of gadolinium based oxide and oxyfluoride glasses as low energy radiation shielding materials. Prog. Nucl. Energy **97**, 53–59 (2017). https://doi.org/10.1016/j.pnucene.2016.12.014
32. I.I. Bashter, Calculation of radiation attenuation coefficients for shielding concretes. Ann. Nucl. Energy **24**(17), 1389–1401 (1997). https://doi.org/10.1016/S0306-4549(97)00003-0
33. M.L. Taylor, R.L. Smith, F. Dossing et al., Robust calculation of effective atomic numbers: the Auto-Z_{eff} software. Med. Phys. **39**(4), 1769–1778 (2012). https://doi.org/10.1118/1.3689810
34. R. El-Mallawany, M.I. Sayyed, M.G. Dong, Comparative shielding properties of some tellurite glasses: part 2. J. Non Cryst. Solids **474**, 16–23 (2017). https://doi.org/10.1016/j.jnoncrysol.2017.08.011
35. P. Kaur, D. Singh, T. Singh, Heavy metal oxide glasses as gamma rays shielding material. Nucl. Eng. Des. **307**, 364–376 (2016). https://doi.org/10.1016/j.nucengdes.2016.07.029
36. N. Chanthima, J. Kaewkhao, Investigation on radiation shielding parameters of bismuth borosilicate glass from 1 keV to 100 GeV. Ann. Nucl. Energy **55**, 23–28 (2013). https://doi.org/10.1016/j.anucene.2012.12.011
37. M.I. Sayyed, Investigation of shielding parameters for smart polymers. Chin. J. Phys. **54**(3), 408–415 (2016). https://doi.org/10.1016/j.cjph.2016.05.002
38. O. Agar, Study on gamma ray shielding performance of concretes doped with natural sepiolite mineral. Radiochim. Acta **106**(12), 1009–1016 (2018). https://doi.org/10.1515/ract-2018-2981
39. http://skuld.bmsc.washington.edu/scatter/AS_periodic.html. X-ray Absorption Edges (2018). Accessed 15 Sept 2018